Mechanical Response of Hybrid Cross-Linked Networks to Uniaxial Deformation: A Molecular Dynamics Model

ARTICLE *in* MACROMOLECULES · DECEMBER 2014

Impact Factor: 5.8 · DOI: 10.1021/ma501504z

4 AUTHORS:

Jan Zidek

Brno University of Technology

21 PUBLICATIONS **22** CITATIONS

SEE PROFILE

Josef Jancar

Brno University of Technology

103 PUBLICATIONS **1,403** CITATIONS

SEE PROFILE

Andrey Milchev

Bulgarian Academy of Sciences

237 PUBLICATIONS **4,464** CITATIONS

SEE PROFILE

Thomas Vilgis

Max Planck Institute for Polymer Research

389 PUBLICATIONS **4,260** CITATIONS

SEE PROFILE

Macromolecules

Article

pubs.acs.org/Macromolecules

Mechanical Response of Hybrid Cross-Linked Networks to Uniaxial Deformation: A Molecular Dynamics Model

Jan Zidek,*[,†] Josef Jancar,[†] Andrey Milchev,[‡] and Thomas A. Vilgis[§]

[†]Central European Institute of Technology; Brno University of Technology, Technicka 10, 616 00 Brno, Czech Republic

[‡]Institute for Physical Chemistry, Bulgarian Academy of Sciences, 1113 Sofia, Bulgaria

[§]Max-Planck Institute for Polymer Research, Ackermannweg 10, 55128 Mainz, Germany

Supporting Information

ABSTRACT: Networks combining physical and covalent chemical cross-links can exhibit a large amount of dissipated inelastic energy along with high stretchability during deformation. We present our analysis of the influence of the extent of covalent cross-linking on the inelasticity of hydrogels. Four model networks, which are similar in structure but strongly differ in elasticity, have been studied. The aim was the identification of a key structural factor responsible for observing a hysteresis or an elastic deformation. In the employed molecular dynamics study this factor is derived from the underlying structure of each particular hydrogel network. Several structural characteristics have been investigated like the extent of damage to the network, chains sliding, and the specific properties of load-bearing chains. By means of such a key factor, one can predict the deformation behavior (hysteresis or elasticity) of some material, provided a precise description of its structure exists and it resembles any of the four types of a network. The results can be applied in the design of bio-inspired materials with tailored properties.

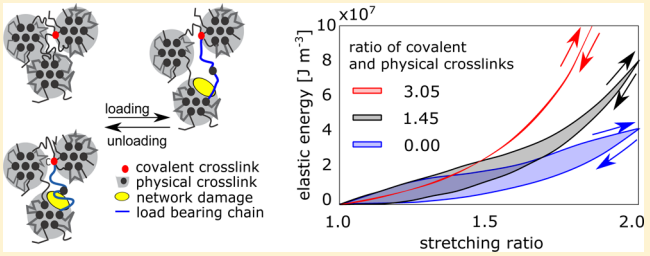

INTRODUCTION

Hydrogels represent a broad range of polymeric materials which are defined as two- or multicomponent systems consisting of at least one three-dimensional polymer network and water as solvent.[1] Their mechanical properties are influenced by a set of structural variables reflecting the properties of the underlying macromolecular networks as well as the solvent and external conditions like pH and temperature. The development of hydrogel materials requires detailed knowledge of relations between physical properties and hydrogel structure.[2−7] In the recent years, double-network hydrogels attracted significant attention due to their excellent mechanical performance compared to traditional hydrogels.[8−11] The term double-network hydrogels refers to networks with two types of covalent cross-links and usually combining two networks of different molecular structure.[8,12] Recently, it has been shown that similar behavior exists in a single polymer network hydrogels with two types of cross-links. The polymer networks investigated in this paper are flexible chains cross-linked with a combination of physical and covalent joints termed hybrid cross-link networks.

We focus on a hysteresis, observed during the mechanical loading−unloading cycle, and, more specifically, on the deformation behavior analogous to the Mullins effect (ME).[13] The ME implies that the deformation behavior depends on the maximum stretching ratio reached over the entire deformation history. The interpretation of such an effect in the literature is still ambiguous. One of the reasons is that the materials, which differ in the extent of hysteresis, differ significantly also in molecular structure. It is difficult to change one structural parameter in the experimental work while preserving the other structural factors.

In order to elucidate this problem, we examine four model networks, with almost identical molecular structure. Upon deformation, one of them exhibits significantly different hysteresis than the three others. We demonstrate that one can find a fundamental structural factor, responsible for the hysteresis in such set of model networks. Only few analogous studies of structurally similar materials can be found in the literature. For example, in networks of alginate/polyacrylamide (PAA) the difference in structure is negligible, if distinct ions with the same charge are replaced, e.g., Ca^{2+} by Sr^{2+} (or by Ba^{2+}). In contrast, the resulting difference in deformation response (hysteresis) is rather significant.[14] This concerns the energy consumption after loading/unloading in four loading cycles: Ca-alginate/PAA > Sr-alginate/PAA. The networks Ca and Sr have very similar elastic modulus. The difference lies probably in the higher mobility of Ca ions compared to Sr, which gives the Ca network more elastic response to deformation. Schmoler and Bausch[15] presented different hysteresis in a biopolymer filled with nanoparticles of austenite and martensite. Both nanoparticles have the same composition

Received: July 22, 2014
Revised: November 19, 2014
Published: December 10, 2014

   dx.doi.org/10.1021/ma501504z | Macromolecules 2014, 47, 8795−8807

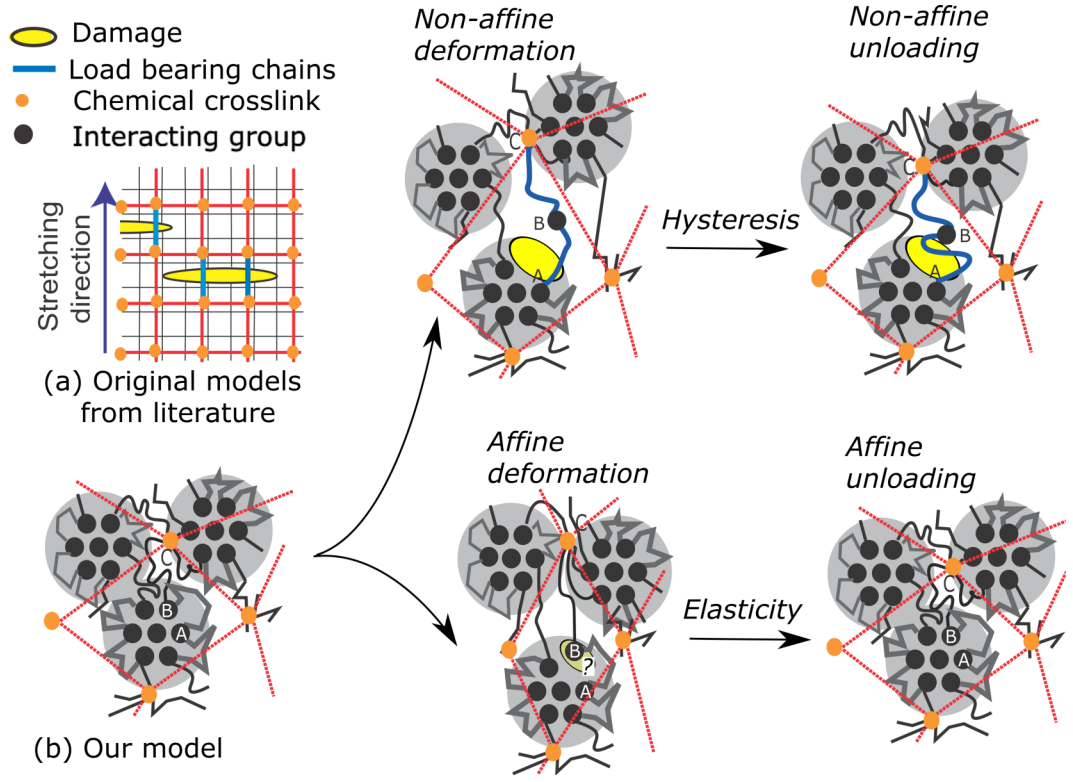

Figure 1. (a) Recent models of double-network gels presented in the literature. (b) Our models structure: ABC-load-bearing chains bridging the damaged zone; two modes of structure evolution during the loading/unloading cycle and their assumed relation to the type of deformation.

and size since the austenite−martensite transition has been induced directly in the material. They differ only in the shape of nanocrystals; nonetheless, they exhibit very different hysteresis. In addition, the motion of cubic crystals of austenite is more restricted than the motion of the rodlike martensite crystals. That is why the network with austenite shows larger hysteresis than martensite.

Our double networks are hybrid networks combined from a physical (i.e., hydrogen bonds) primary network and a covalently cross-linked secondary network. Such hybrid cross-linked networks are frequently reported in the literature.[16,17] Typical for such materials is the change of the physical network during the additional covalent cross-linking. So Li et al.[18] reported the cross-linking of a physical hydrogel by tetraethyl orthosilicate (TEOS). The chemical cross-linking leads to the formation of silicon dioxide in the gel phase. The network softening, caused by additional cross-linking, was observed also in a work by Costa et al.[19] The articles[13,20] describe the Mullins effect as changes in the structure induced by the first loading−unloading cycle.

Such structural changes are expected to persist in the material for a long time or even permanently. Therefore, when a material is deformed in the course of many loading−unloading cycles, the first deformation cycle differs from the subsequent ones. However, not every hydrogel network that exhibits a hysteresis shows also the Mullins effect (ME). Gels with hysteresis, yet without ME, have probably a quick structural recovery after each deformation cycle. The second cycle can have then a hysteresis, too, but it follows the first one as in the case of alginate hydrogels.[14] Among the hydrogels, where the ME has been found, are for example gels from 2-acrylamido-2-methylpropanesulfonic acid[20] and poly(*N*-isopropylacrylamide) (PNIPAAm).[21]

It is a serious challenge to fully understand these phenomena through experimental techniques. Thus, equilibrium coarse-grained MD simulations were performed to provide at least qualitative relationships between structure and deformation properties.

Theoretical models can give complementary information about the relationship between structure and properties. They mimic some structural phenomena, observed during deformation, that cannot be analyzed by experimental work. The models describing the mechanical properties of double network[22−25] consider the material as a combination of a primary dense network and a secondary network, which is less dense. The primary network is brittle itself while the secondary one is stable and robust. The schematic picture of the existing models is presented in Figure 1a. The primary network is symbolized by black lines and the secondary one by an orange network. These models ascribe strain softening to the formation of cracks in primary polymer network. The damaged zone is presented as yellow object in Figure 1. Other published models encompass the role of chains of the secondary networks as bridging the damaged zone of primary network (blue chains). Such models provide information about the dynamic development of bridging chains[26,27] during deformation. These models provide also information about the structural changes during deformation. Our molecular model is based on the existing models of double-network hydrogels.

The description[22−232425] does not correspond to the behavior of hydrogels as the damage of primary network in the hydrogels does not have a character of a crack. Our models (Figure 1b) are better suited to describe a real hydrogel network structure than the aforementioned models, as they consider the physical cross-links as clusters of interacting groups. The physical clusters are connected by flexible chains.

dx.doi.org/10.1021/ma501504z | *Macromolecules* 2014, 47, 8795−8807

The self-assembly of physical connections is frequently observed in biological systems. Peleg et al.[28] describe the unfolding of physically interacting clusters, which are similar to the physical cross-links (PCLs) in our model. The dissociation of physical clusters is responsible for the dynamic deformation response of the material. The structure of folded proteins from the model of Peleg differs from that in hydrogels. The hydrogels have secondary structure of entangled network. The damage in our hydrogel models is modeled as a dissociation of the interacting groups from the existing physical cross-links.The damage after dissociation is highlighted by yellow ellipse in Figure 1.

Also, the load-bearing chains are treated in the mentioned models as chains which bridge the damaged zone whereas our models make possible to detect the load-bearing chains on the molecular scale (Figure 1b, chain marked by letters ABC). We can describe the evolution of load bearing chains during loading and analyze them in the simulation.

The model proposed in this work has also an additional advantage in describing hybrid networks since the existing theoretical models cannot distinguish between hybrid networks and interpenetrating polymer networks (IPNs). Indeed, hybrid networks combine physical and covalent cross-links in a single network while the IPNs are composed of two interlaced networks. Our molecular model can distinguish between these two types of structures.

MODELS AND METHODS

The models described here are based on our previous model of a physically cross-linked network,[29] swollen in water, which was subsequently covalently cross-linked. We focus on hybrid networks because we can thus study a double network *without* a significant modification of the structure of physical networks. The underlying idea thereby is the distinction between two modes of network evolution: an affine and nonaffine deformation. Each mode leads to a different mechanical response: the nonaffine to hysteresis and the affine to elasticity (Figure 1). The deformation with hysteresis is accompanied by dissociation of AA groups in structure. During the reverse deformation, such group is not fully reassociated with the cluster and a hysteresis is observed (Figure 1). The elastic deformation response is associated with affine deformation. In that case, the interacting atomic group is attached to the cluster during loading and unloading cycle (Figure 1). The degree of covalent cross-linking is considered as a crucial factor during network evolution. The data from simulations, however, indicate that the real mechanisms of elastic or inelastic behavior are more complex than those sketched in Figure 1. We focus on different model aspects: network damage, load-bearing chains, and the detailed evolution of structure. From the simulation data we determine which structural aspects render the behavior of a material elastic or inelastic.

Generally, one can see a hysteresis when the structure changes as a function of time. In the present investigation we took the density of configurational energy as an appropriate function that reflects the changes in hydrogel structure. Therefore, we integrated the stress−strain curves of loading/unloading, obtained in the present work, and calculated the consumed energy density. Our model networks exhibit a hysteresis only in the ME regime whereby the recovery of the structural changes is relatively slow in comparison to the rate of deformation. During this time, we can control the structure with respect to hysteresis/elasticity. However, we are not able to govern the switch of deformation response between ME/non-ME type of hysteresis.

We performed a large amount of simulations of networks with varying number of covalent bonds (between 0 and 128) in the simulation box. The deformation response of very lightly cross-linked network with up to 8 covalent bonds per simulation box was almost identical to the response of physical networks. The deformation response of the networks in the interval from 64 to 128 was elastic, and the stiffness of the network steadily increased along with the increased covalent cross-link density.

To elucidate the observed differences in network behavior, we have defined four principal model cases in the present investigation (cf. Table 1), depending on the number n_{cov} of covalent cross-links in the box. This single model parameter was recalculated to the structural parameter *cpc*, which will be described below. The parameter *cpc* reflects the degree of physical and covalent interaction in the box and describes adequately the character of network.

Table 1. List of Networks Applied in This Paper: Name of Model, Parameter *cpc*, and Number Covalent Cross-Links per Box n_{cov}

model	*cpc*	model name	n_{cov}
I	0.00	physical network	0
II	0.70	lightly covalently cross-linked	16
III	1.45	moderately covalently cross-linked	32
IV	3.05	strongly covalently cross-linked	64

Model of Physically Cross-Linked Network Hydrogels.

Our original model network,[29] which we extend in this work, has been designed to simulate the structure of hydrogels with physical cross-links (PCLs) in the form of acrylic acid (AA) clusters. The clusters are objects composed of several AA groups concentrated in small volume. They are detected by the cluster counting algorithm. The algorithm uses single linkage (nearest neighbor) clustering method integrated in MATLAB software. The linkage of a particular AA group to a cluster is established, when the nearest distance to the neighbor AA group from the cluster is less than or equal to the cutoff distance (0.35 nm). This network has been used as a limiting case of physical network with zero degree of covalent cross-linking. The model was designed so as to mimic a real chemical structure of poly(ethylene glycol) (PEG) gel cross-linked by polylactide glycolide micelles of (PLGA) and acrylic acid (AA). In fact, real hydrogels are mostly composed of micelles. The real micelles are reduced in our models to the minimalistic structure of interacting clusters of AA, which create a core of micelles (Figure 2b). As output from the simulation one gets then a set of atomic coordinates visualized using the VMD software.[30] The atomistic configuration of purely physical network model is presented here in Figure 2.

The atomistic configuration from Figure 2 corresponds to the schematic picture of Figure 1b. The first snapshot in Figure 2a shows the dry phase consisting of all components. The solvent is not shown. The blue interacting groups of acrylic acid (AA) are assembled into clusters. They are schematically depicted as black circles in Figure 1. The next structural components are shells around the physical clusters. The schematic Figure 1b shows the micelles including shells as gray objects. Their real shape is shown in Figure 2b, where yellow chains stand for the shells. The clusters are connected by

dx.doi.org/10.1021/ma501504z | *Macromolecules* 2014, 47, 8795−8807

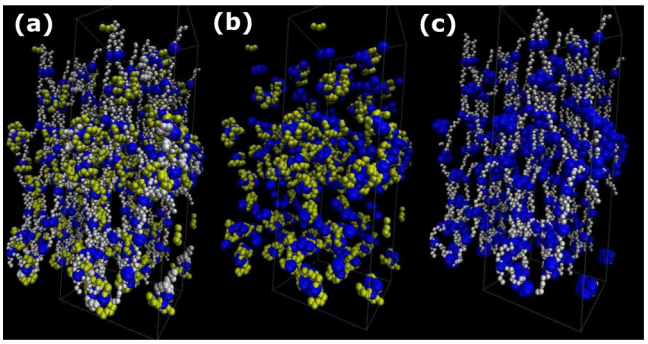

Figure 2. Visualization (a) of a physical network [without solvent for better visibility], highlighting (b) some typical model parts: core (blue)−shell (yellow) structure of physical clusters (PCLs). (c) Load-bearing chains (white) connecting the physical clusters. See the Supporting Information for more pictures: box with solvent; stereoscopic 3D anaglyphs (with red cyan glasses), 3D Vision Live ready files (with stereoscopic glasses).

flexible chains, which are presented as black lines in Figure 1b. In the snapshots, they are described as white objects in Figure 2c.

The simulation box contained 1600 atomic groups of organic phase (in Figure 2a) and 2447 molecules of water. Configurations with water are displayed in the Supporting Information. The organic phase was composed of 160 interacting groups of acrylic acid AA and 1440 atomic groups of flexible chains of poly(ethylene glycol). The water molecules were modeled using the standard simple point charge (SPC-E) model of water.[31]

The atomic configuration from Figure 2 was spontaneously formed from our original generic model. The original model was without physical interaction, i.e., without physical cross-links (PCLs) between AA groups and physical clusters. Thus, the structure of the original model was an entangled network without physical cross-links. The clusters of AA groups (PCLs) were formed owing to the interaction between AA groups. The formation and destruction of of AA cluster are reversible with switching (on/off) of the physical interactions.

The flexible chains were taken as artificially entangled and periodic. This represents the situation when the realistic size of macromolecules is significantly longer than the linear size of the simulation box (5 nm). The macromolecules of PEG with low molecular weight have M_w = 1000 g mol^{-1}; the length in the stretched state is approximately 7 nm.

One macromolecule was composed of 200 atomic group with repeating sequence -AA-CH_2-CH_2-O-CH_2-CH_2-O-CH_2-CH_2-O, where AA is acrylic acid represented by single bead, CH_2 is methylene group, and O is oxygen atom. The initial macroscopic concentration of all atomic groups in the simulation box before equilibration was taken as uniform.

The network deformation was modeled by means of molecular dynamics using the GROMACS software package[32] with velocity rescaling thermostat.[33] The particular velocity-rescaling thermostat is an extended Berendsen thermostat. As the Berendsen thermostat, the V-rescale thermostat corrects the deviation of the actual and setup temperature. Then the velocities are rescaled so that the total kinetic energy is conserved. The velocities should have realistic Gaussian and stochastic distribution. The next, Nosé−Hoover, thermostat has a chain of virtual particles with certain kinetic energy. The length of the chain (number of chained Nosé−Hoover virtual particles) is an additional parameter of the thermostat. The recommended chain length is at least 3−4 particles.

We tested two thermostats: velocity rescale and the Nosé−Hoover thermostat with default settings in GROMACS (10 particles). We selected the velocity rescale thermostat. It can produce canonical ensemble, while the oscillations of temperature are decreased.

The initial simulation box was a cube with 5 nm side length. The box was deformed at deformation rate of 0.1 ns^{-1} along the z-axis. Along the x (y)-axis, the model box was compressed in order to keep the volume constant. The energy density W was recorded during the simulation for the follow-up calculation of the stress−strain function: $\sigma = \lambda_z(\partial W/\partial\lambda_z) - \lambda_{xy}(\partial W/\partial\lambda_{xy})$, where λ is the extension ratio along the respective axis.

The model network showed hysteresis effects, indicating a softening phase during the deformation. The softening phase was caused by damage of the physical network. The analysis of network was performed predominantly in the stretched state (Figure 2). For example, the load-bearing chains were identified from the simulation box. The scans of energy and structural analyses were calculated as an average from four independent simulations with the same degree of cross-linking and different initial coordinates of atomic groups.

Additional Covalent Cross-Linking. The network from the previous section was transformed to the hybrid physical/covalent networks. The covalent cross-links (CCL) are modeled as additional bonding interaction between neighboring chains with a bond strength equal to that of the chain. The main (user defined) parameter was a number of CCLs in simulation box (n_{CCLs}). Covalent cross-links were added between the closest segments of two neighboring chains (intrachain CCLs were not considered so that the original structure of the physically cross-linked network remained largely unchanged). The atomic pairs for creation of CCLs were supposed to meet three conditions. (i) The original atomic groups of pairs before connection must be at distances less than 0.4 nm. (ii) They should belong to different macromolecular chains to prevent formation of chain loops. (iii) A cross-link is allowed only between two carbon atoms from a PEG chain. Thus, oxygen atoms and AA groups were excluded from creating a covalent cross-link.

The main structural parameter was the ratio of the number of covalent cross-links (or n_{CCL}) relative to the number of AA clusters n_{PCL} in the simulation box. It is abbreviated as *cpc* (covalent/physical cross-link ratio) in the entire paper:

$$cpc = \frac{n_{CCLs}}{n_{PCLs}} \quad (1)$$

This ratio makes it possible to compare a broad range of covalently and physically cross-linked structures in the simulation box and is itself independent of the simulation box size. The PCLs were formed spontaneously, and their number cannot be controlled. However, their number varies slightly, when the networks have the same parameter *cpc* ($\Delta n_{PCL} = \pm 1$).

Following the definition of four principal cases of network (Table 1), the value of *cpc* for the different network types in our simulations ranged from a purely physically cross-linked network, *cpc* = 0, through lightly covalently cross-linked networks, *cpc* = 0.7, to moderately covalently cross-linked network, *cpc* = 1.45, up to predominantly covalently cross-linked network with *cpc* = 3.05. Although the CCLs were formed randomly, they mostly appeared in vicinity of PCL. So a

dx.doi.org/10.1021/ma501504z | Macromolecules 2014, 47, 8795−8807

structural component PCL/CCLs was defined. Such combined structural components were marked as hybrid cross-links, which enabled us to define the four structural types of networks from Table 1:

- *Physical network* contains physical cross-links (PCL) only and no hybrid (CCL/PCL) cross-links. It displays a deformation of a physical type of network with softening phase.
- *Lightly covalently cross-linked network* has the number of covalent cross-links lower than the number of physical cross-links in the original network, $n_{CCL} < n_{PCL}$. So, the network is a mixed type of both physical cross-links and hybrid (CCL/PCL) cross-link. The network still resembles a physical type of network. However, at this concentration the CCLs begin to have an effect on the deformation properties which in networks with $cpc < 0.7$ were similar to purely physical network.
- *Moderately covalently cross-linked network* with $cpc = 1.45$ has $n_{CCL} > n_{PCL}$. In fact, almost all cross-links are just hybrid PCL/CCL. As the CCLs are distributed unequally, a network with slight excess of CCLs ($cpc = 1.45$) is representative. According to the deformation properties, the network is supposed to be between physical and covalent type of network.
- *Strongly covalently cross-linked network* ($cpc = 3.05$) has significant excess of CCLs, and all PCLs are accompanied by one or more covalent cross-links. It is unambiguously a covalent type of network also from the point of view of deformation behavior.

Detection of Nonaffinity Degree and Network Type. The extent of nonaffine deformation is another structural factor that provides valuable information during network deformation. It indicates how the deformation of individual components corresponds to the macroscopic deformation of the sample. The method for calculating the degree of nonaffinity has been presented earlier.[34−37] We selected a network reconstruction parameter V according to Kurniawan[38] as a criterion of nonaffinity:

$$V = \langle |\mathbf{u} - \mathbf{u}^{aff}| \rangle \tag{2}$$

where $\mathbf{u}$ denotes the actual real displacements of cross-links, derived from the MD simulation, and $\mathbf{u}^{aff}$ are the respective imaginative affine displacements. Zero value of V means, therefore, a fully affine deformation. A high value of V, in contrast, indicates a nonaffine deformation. The parameter V can be calculated for any selection of atomic groups in the simulation box. Particularly, it has been calculated for physical cross-links (PCLs) and for covalent cross-links (CCLs).

We assume that one of the groups (PCLs or CCLs), which is more affine, acts as network node. The ratio V_{CCLs}/V_{PCLs} was calculated and taken as an indicator of the type of cross-link dominating the network. For $V_{CCLs}/V_{PCLs} > 1$, the network is dominated by AA clusters, and the network behaves as a physically cross-linked one. For $V_{CCLs}/V_{PCLs} < 1$, in contrast, the more affine components are the covalent cross-links, and the network behaves as a covalently cross-linked one.

Detection and Analysis of Load-Bearing Chains. Existing theoretical models consider load-bearing chains of the secondary network as bridging the damaged zone. In our approach, the load-bearing chains are the chains bridging two physical clusters (PCLs), or covalent cross-links (CCLs), or a PCL and CCL in a stretched state. The load-bearing chains are detected in the simulation box in a stretched state (Figure 2a). The chain ends are always either physically interacting (AA) groups, present in the PCL, or covalent cross-links (CCLs). Other atomic groups such as carbonyl (CH_2), oxygen (O), and the acrylic acid (AA) groups *outside* PCLs cannot be set as chain ends.

Two types of chains were excluded (marked as non-LBC) from the set of LBC: (i) Chains, which begin and end in the same cluster. Such chains create shells around physical clusters (highlighted yellow in Figure 2b). (ii) If a chain between CCL and PCL happens to be too short (i.e., has fewer than four atomic bonds), it is not counted as LBC either. In that case, the CCL is in the vicinity of PCL, and they form a complex object—a hybrid physical/covalent cross-link.

The chains remaining after the exclusion of the aforementioned chains were considered load-bearing chains. They had variable chain length in the range from 5 up to 31 successively connected atomic beads (i.e., from 4 bonds to 30 bonds, respectively). They are shown in Figure 2c as white chains. Each chain has two characteristic parameters: a contour length and a number of segments. Both parameters were calculated from chain geometry in the fully stretched state. The contour length of a chain (l_c) was calculated as the length of a fully stretched molecular chain. The number of segments ($N_s = l_c/(2l_p)$) was derived from the model persistence length (l_p), selected as 0.1 nm. This model value is significantly lower than the value of real PEG (0.38 nm). This model value was used because the model chains were shorter than the usual chains in real materials. However, the deformation response of the model chains corresponds to the response of rubbery chains. The variable property of each LBC at given time during the simulation was the end-to-end length l_e. It is related to the elastic energy according to Treloar:[39]

$$W = N_s kT\left\{l\beta(l) + \ln\left[\frac{\beta(l)}{\sinh \beta(l)}\right]\right\} \tag{3}$$

where N_s is the number of chain segments, $l = l_e/(l_c\sqrt{N_s})$, and kT is the thermal energy per segment. The quantity β is calculated as the inverse Langevin function: $\beta = \mathcal{L}^{-1}[l_e/(l_c\sqrt{N_s})]$, where the Langevin function itself reads $\mathcal{L}(x) = \coth x + x^{-1}$.

Continuity of Networks of Covalently Cross-Linked (CCLs). A continuous CCLs subnetwork is a subset of all CCLs in the simulation box. It is created by elastic chains interconnected by covalent cross-links (CCLs) only. In such a subnetwork it must be possible to tread between two CCLs only through elastic chains, or other CCLs. In the case when all the paths are disjointed by PCLs, there is no continuous connection whatsoever. The continuity of a given network was analyzed by means of the Floyd−Warshall algorithm.[40,41] The algorithm is designed to search for the shortest path between two vertices in a network graph. However, it can also detect whether a continuous path spans any two vertices in a given network. Our application of the algorithm investigates the network of covalent cross-links (CCLs). The input for the algorithm is an indexed matrix of covalent cross-links (for example Figure 3, index 1−5). Another input variable is a table of chains connectivity. A continuous path means that it is possible to tread from the starting cross-link to some terminal covalent cross-link only through elastic chains and covalent cross-links. Figure 3a shows a path where all the CCLs are connected into a single subnetwork. Even if the nodes 1 and 2 are disjointed by PCL, it is still possible to pass through the points 3 and 4. The Floyd−Warshall algorithm yields a distance matrix $\mathbf{D}$ of pairs of covalent cross-links in eq 4. Since all the

dx.doi.org/10.1021/ma501504z | Macromolecules 2014, 47, 8795−8807

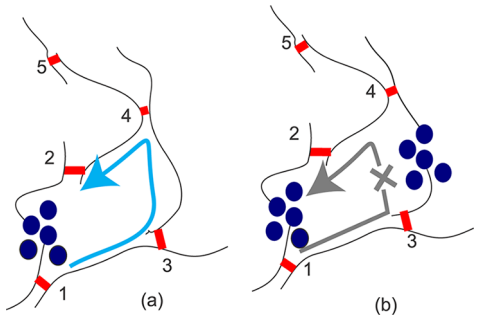

Figure 3. Sketch of a covalently cross-linked (CCLs) network continuity; red lines = covalent cross-links (CCLs), blue circles = physical cross-links (PCLs): (a) all CCLs are connected into a single continuous subnetwork; (b) subnetworks of cross-links are interrupted by PCLs.

cross-links are connected to one segment of covalent network, the network does not contain the ∞ sign which signals a cut (interrupt). There is also no need to transform this matrix. The block of these CCLs is described by the entire matrix.

$$\mathbf{D} = \begin{pmatrix} 0 & 3 & 1 & 2 & 3 \\ 3 & 0 & 2 & 1 & 2 \\ 1 & 2 & 0 & 1 & 1 \\ 2 & 1 & 1 & 0 & 1 \\ 3 & 2 & 1 & 1 & 0 \end{pmatrix} \quad (4)$$

The network in Figure 3b is different. Each element of the matrix $\mathbf{D}_{ij}$ stands for the total number of elastic chains connecting the CCLs with index i and j. Alternatively, the element may have an "infinite" value (in analogy with infinite resistance), when a continuous path between two cross-links is absent. The **D** matrix, corresponding to Figure 3b, has been eventually transformed into a block-diagonal form:

$$\mathbf{D} = \begin{pmatrix} 0 & \infty & 1 & \infty & \infty \\ \infty & 0 & \infty & 1 & 2 \\ 1 & \infty & 0 & \infty & \infty \\ \infty & 1 & \infty & 0 & 1 \\ \infty & 2 & \infty & 1 & 0 \end{pmatrix} = \begin{pmatrix} 0 & 1 & \infty & \infty & \infty \\ 1 & 0 & \infty & \infty & \infty \\ \infty & \infty & 0 & 1 & 2 \\ \infty & \infty & 1 & 0 & 1 \\ \infty & \infty & 2 & 1 & 0 \end{pmatrix} \quad (5)$$

Each block in the matrix contains a $n \times n$ square submatrix, and each square represents a system of n cross-links, interconnected by covalently cross-linked network. In the particular case of Figure 3b, the system contains one subnetwork of two cross-links and a second subnetwork of three cross-links.

RESULTS AND DISCUSSION

The models of hybrid networks, examined in the present study, were derived from the models of physically cross-linked gels, which we investigated recently.[29] It was found that both model and real materials show softening and hysteresis during deformation.

An open question, however, is whether the hysteresis is related to the Mullins effect. The previous examples from literature[20] indicate that some of the double network hydrogels indeed exhibit ME. The ME is usually revealed by a special type of experiment with multiple loading/unloading cycles. The network is deformed in each successive cycle beyond what was reached in the previous one. In each new cycle the loading curve has two parts. It follows the previous unloading curve until the maximum elongation reached in the preceding cycle is attained. Above such maximal deformation, it follows the basic curve of the direct deformation (Figure 4a, blue curve). Figure 4a shows an analogous cyclic deformation response of physical model network with $cpc = 0$. The only difference with respect to real double-network hydrogels is that here the elastic energy density ΔW was calculated instead of the stress. Apparently, the cyclic deformation manifests the "Mullins effect" in our model hydrogel, too.

Schematically, this mechanism is presented in Figure 4b. The model indicates that a zone of damage appears in state II, reached in the first cycle of stretching deformation. However, this zone does not vanish after unloading (in state III). During the next cycle, the damage even increases (state V) and does not vanish after repeated unloading (phase VI) either. Such a mechanism complies with the basic idea of the Mullins effect in hydrogels. Moreover, the damage should be different in the networks with hysteresis and in elastic networks.

According to our observations, all networks with hysteresis (lightly and moderately covalently cross-linked networks) exhibit a "Mullins effect" behavior, too. On the other hand, with increased degree of covalent cross-linking, the network resembles structurally more and more a covalent (elastic) network. It has been presumed, therefore, that the additional covalent cross-linking would inhibit the hysteresis and suppress the Mullins effect. In our simulations, the degree of covalent cross-linking was systematically increased and the hysteresis during deformation was monitored in the different networks.

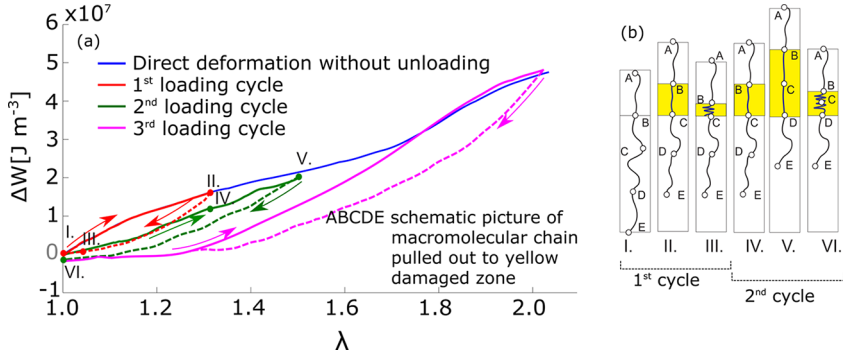

Figure 4. (a) Elastic energy of a physical gel ($cpc = 0$) during multiple loading–unloading deformations in the regime of the Mullins effect. Solid lines denote stretching; dashed lines stand for unloading. (b) Pulling out a chain of segments A–B–C–D–E, which undergoes damage (yellow). Roman numbers mark deformation states during different cycles. The points B–C–D denote load-bearing chains during multiple cycles.

dx.doi.org/10.1021/ma501504z | Macromolecules 2014, 47, 8795–8807

The hysteresis disappeared when the concentration of covalent cross-links reached approximately 3 CCLs per one PCL (*cpc* = 3.05, strongly cross-linked network, Figure 5). However, the

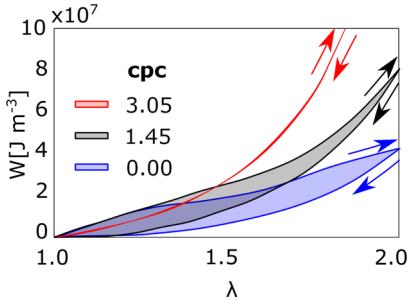

Figure 5. Energy density as a function of stretching ratio λ from a single forward−reverse deformation: a moderately cross-linked network with *cpc* = 1.45 still shows a hysteresis as that with *cpc* = 0; the strongly cross-linked *cpc* = 3.05 network is elastic.

other explored networks up to moderately cross-linked network *cpc* = 1.45 manifest deformation behavior *with* hysteresis, similar to the physical network with *cpc* = 0. So, the network with *cpc* = 1.45 exhibits a hysteresis which occurs in the same range of deformation λ as in the purely physical network with no CCLs. Moreover, both PCL- and CCL-type cross-links are still present even in the network with *cpc* = 3.05, whereby the PCLs persist there almost in the same concentration as in the network with *cpc* = 0. Thus, the rapid change of network structure (i.e., by varying the type of cross-links) does not immediately govern the deformation behavior of the networks.

Visually, the network structure changes gradually with increasing the number of covalent cross-links yet is not distorted.

The differences can be highlighted when we focus on hybrid PCL/CCLs cross-links. We mark purely physical cross-link in blue (Figure 6) and hybrid physical cross-link with covalent cross-links in their vicinity in green. The snapshots are presented in the Supporting Information. However, in the case of hysteresis and elasticity, the boundary between inelastic and elastic behavior is in the interval, where the networks are very similar.

Structural Interpretation of the Hysteresis. In this section we examine the principal reasons for the existence of hysteresis and Mullins effect in a network which has been discussed in the literature recently. Generally, the Mullins effect is believed to be caused mainly by bond rupture, disentanglement, and polymer chain sliding.[13]

The first of these structural properties is bond rupture and/or disentanglement. Such factors are merged into a single model factor in our study—a network damage. Thereby, damage of the secondary network is suppressed in our models since the model setup enables neither bond rupture nor disentanglement in the secondary network.

The damage in the primary network is modeled in this case as dissociation of interacting groups from the existing physical cross-links. The volume fraction of physical cross-links (PCLs) has been determined in the simulation box as a function of deformation. The schematic idea of this mechanism is presented in Figure 7b. It was expected that this kind of damage will vary with increasing degree of covalent cross-linking. In the most strongly cross-linked network, the damage is expected to be different in its nature. Moreover, it should

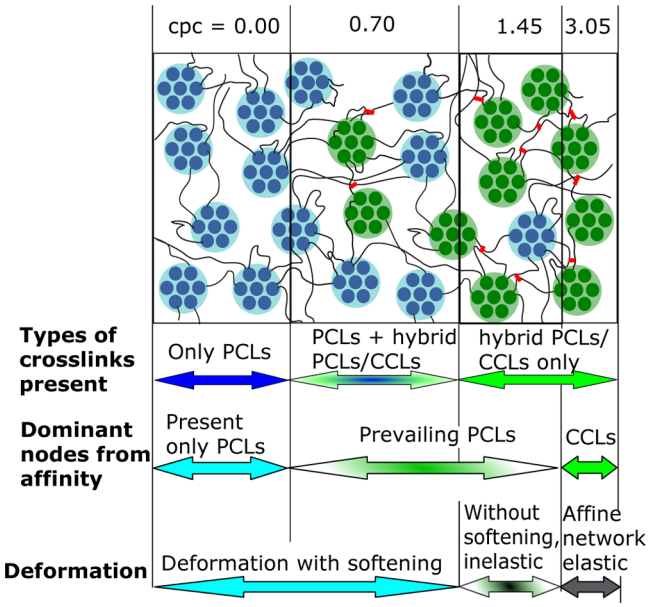

Figure 6. Schematic structure of hybrid networks as a functions of concentration of covalent cross-links: blue = physical cross-links (PCL); red = covalent cross-links (CCL); green/red = hybrid PCL/CCL; black = flexible chains. The type of cross-links is compared to the type of deformation and type of dominant cross-links according to the affinity.

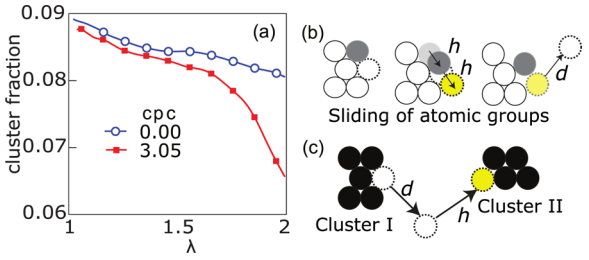

Figure 7. (a) Volume fraction of physical cross-links as a function of the stretching ratio λ for the network without covalent cross-linking and for a strongly cross-linked one. Damage *d* is defined as a decrease of PCLs volume fraction during deformation. (b, c) Two types of network healing *h* are observed: (b) reconstruction of clusters and (c) segmental hops from one to another cluster.

quickly vanish during the subsequent unloading phase. The cluster fractions were compared in two limiting cases for a physical *cpc* = 0 and for a strongly covalently cross-linked network with *cpc* = 3.05 (Figure 7). In the first phase of the deformation until λ = 1.6, the fractions of PCLs were very close. They differed significantly at large deformation only whereas the hysteresis differs already from the very onset of the deformation.

We know from the previous analysis that the energy gain of attachment of an interacting group to a cluster is higher for the case of physical, lightly, and moderately cross-linked network (*cpc* $\leq$ 1.45) than in a strongly cross-linked network (*cpc* = 3.05). The reason for such difference is the significantly stronger force acting on AA groups in a cross-linked network. When the force is acting on a physically attached object, the energy barrier is decreased. The energy of attachment of AA group is shown in Figure 8a. As a result, the AA group is attached strongly in physical networks and weakly in a covalently cross-linked network (Figure 8b). Here E_A is the

dx.doi.org/10.1021/ma501504z | Macromolecules 2014, 47, 8795−8807

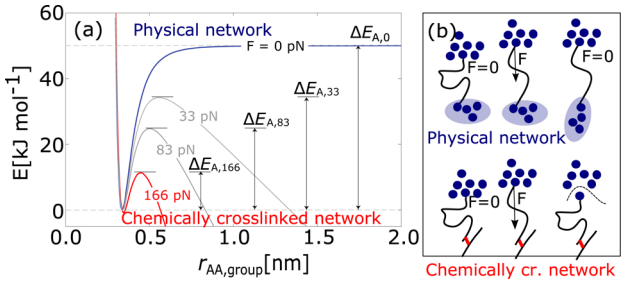

Figure 8. (a) Energy barrier for attachment of an interacting AA group to a cluster; the interacting group is loaded by a force (numbers at lines); ΔE_A = activation energy of attachment of an AA group. (b) Top: the chain attached by physical cross-links from left to right: unstretched, stretched, and response of PCL to stretching. Bottom: chain attached by covalent cross-link; unstretched, stretched, and dissociation of AA group.

energy barrier which must be overcome in order to dissociate the interacting group from the cluster (the force strength is indicated by a number at each ΔE_A value in Figure 8b).

Some damage-healing mechanisms exist in networks, depending on whether they are elastic or nonelastic. A self-repairing process is predominantly observed in biomaterials with very complex chemistry and physics. From our data it can be seen that some kind of self-healing can occur also in model materials with simple structure. Moreover, the mechanism can switch between two modes (Figure 7b,c), and the switch between them can be controlled.

In the case of networks with hysteresis, loading of physical cross-links by an external force leads to spatial reconstruction of atomic groups in each cluster (Figure 7b). It is not accompanied by transfer of interacting groups between physical clusters. The cluster reconstruction can have two alternative of mechanisms whereby both are observed. Figure 7b (left) shows a dissociation (d) and an immediate reassociation to the same cluster (r) take place. Alternatively, a sliding of chains past the surface of a cluster (middle picture) may occur. The right picture shows dissociation of atomic group from reconstructed cluster. A mechanism of cluster reconstruction leads to the relaxation of force and so delays the dissociation of AA groups from the interacting cluster. The change in structure takes time, and the overall response is inelastic.

On the other hand, in the case of strongly covalently cross-linked network with *cpc* = 3.05, the atomic group is more easily dissociated from the cluster. The same or another atomic group is thereby immediately reattached to another cluster (Figure 7c). Both the dissociation (d) from cluster I and reattachment to the cluster II (h) are in that case very fast. Such structural change is nearly instantaneous and so an elastic response is observed. The process of segmental hops does not have influence on the potential energy. The initial and final states are energetically similar.

Thus, the network response is controlled by two different healing modes, albeit both of them have finally a similar effect on the eventual amount of damage.

Another mechanism that leads to the Mullins effect is sliding of macromolecules relative to one another. One can imagine that the sliding of highly covalently cross-linked chains will be suppressed in comparison to covalently un-cross-linked ones. Such sliding is related to the affinity of deformation. Therefore, we compared the affinities in the limiting cases of physical (*cpc* = 0) and in strongly covalently cross-linked (*cpc* = 3.05) networks in order to check whether the Mullins effect can be caused by sliding of molecules. The network reconstruction parameter V from eq 2 was used as a quantitative criterion of nonaffinity (Figure 9a). The nonaffinity of a physically cross-linked network is slightly higher than for covalently cross-linked network. However, the difference is not sufficient to be considered as governing the change in deformation behavior.

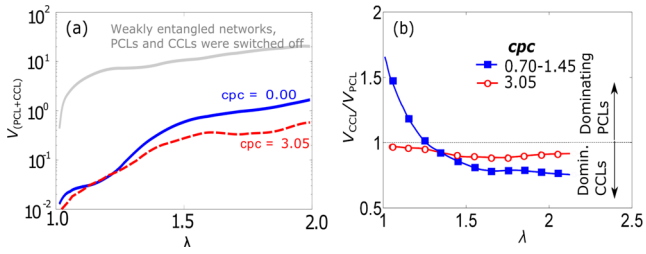

Figure 9. (a) Network reconstruction parameter as a function of the stretching ratio of the simulation box for a physical network (*cpc* = 0) and for a strongly covalently cross-linked network (*cpc* = 3.05), showing the relative importance of different types of nodes in the network. If $V_{CCL}/V_{PCL} > 1$, the network is kept together by AA clusters; in contrast, for $V_{CCL}/V_{PCL} < 1$, cross-links dominate. Blue = averaged curve of physical networks; red = covalently cross-linked networks.

Although the overall affinity of network nodes is similar, the affinities of the individual types of cross-links (CCLs and PCLs) can differ significantly. Their ratio reflects the type of network which is prevailing in the actual network model (Figure 9b). The covalent cross-links show higher affinity than the physical ones ($V_{CCL}/V_{PCL} < 1$). In that model network the CCLs dominate. An opposite situation occurs at lower deformation. The PCLs have lower affinity than the CCLs, and so they dominate. At high deformation, $\lambda > 1.3$, the type of network is switched to the network with prevailing CCLs due to a partial destruction of the network composed of physical cross-links that always happens during deformation.

Summarizing, one could claim that the structural changes presented in the literature—bond rupture, disentanglement, and molecules sliding—cannot be used as a criterion for sharp change from inelastic to elastic networks. Only some indirectly derived parameters correlate with the network type, whereby "indirectly" means that they are derived from another structural parameter and not from the immediate atomic configuration in the simulation box. The elastic/inelastic networks differ in the mechanism of network healing, which is derived from network damage. Moreover, the parameter derived from the dominating affinity of the network also correlates with the deformation response. The disadvantage of such parameters, however, is that they are not derived directly from the structure so that relation to the model structure of networks is not clear.

Load-Bearing Chains (LBC). A second basic structural aspect of the double-network gel models concerns the load bearing chains LBC. A basic parameter of such chains is their elongation, that is, the attained end-to-end distance upon stretching.

The load-bearing chain comprises a number of segments and is characterized by a given contour length. The elastic energy of chains stretched to some end-to-end distance was calculated by Treloar's equation (3). The total elastic energy of all load-bearing chains, calculated from the model, is shown in Figure 10. It has been compared to the elastic energy of the entire

dx.doi.org/10.1021/ma501504z | Macromolecules 2014, 47, 8795−8807

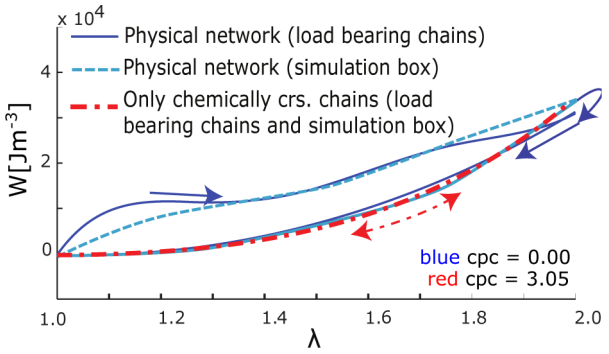

Figure 10. Increase of energy density during stretching of the sample: energy density of load-bearing chains connecting physical cross-links (full line, blue) and load-bearing chains connecting covalent cross-links (dash-dotted line, red). Dashed line stands for the energy density of the whole sample for comparison.

hydrogel in the simulation box. The latter was taken from Figure 5 and rescaled in order to compare the elastic energies from load-bearing chains.

In the case of strongly covalently cross-linked network, the forward and reverse deformations are almost identical. Similarly, the energy density functions from the entire simulation box, and from the elastic chains alone, largely correlate. Thus, one can conclude that in the cross-linked network the behavior is determined by the properties of the elastic load-bearing chains only.

The load-bearing chains exhibit hysteresis as does the entire physically cross-linked network. Only a few differences can be found between load-bearing chains and the entire network. In the initial phase of the deformation, the group of load-bearing chains is stiffer than the entire network. The softening in the load-bearing chains is then more intensive than in the entire network. Probably, the stress acting on LBC is diminished by other network components, for example, by other physical interactions and the rearrangement of water in the simulation box. In the final stage of deformation between λ = 1.8 and 2.0, the total network itself becomes stiffer than the load-bearing chains alone. The remaining (non-LBC) physical interactions still contribute to the resistance in that case.

The deformation response of other (not load-bearing) chains differs from that of the LBC. The response becomes irregular with increasing deformation, but this has a much smaller effect than the change in energy of the load-bearing chains. The functions ΔW in Figure 10 show that there is a strong correlation between the hysteresis of the entire system and the load-bearing chains so that the reason for this has to be identified.

The set of LBC from physical network, as indicated in Figure 10, exhibits a hysteresis upon stretching. In oder to verify if this applies to each chain in particular, we selected a single chain from the physical network and monitored its deformation. The attachments to existing clusters are indicated in Figure 11. In the undeformed state, both ends of a LBC (shown blue in Figure 11) are terminated by physical cross-links. These attachments are progressively destroyed during the deformation. Figure 11 shows such interacting COOH groups, which are either attached to a cluster or free (dangling).

The chain behavior is illustrated by a schematic picture (cf. Figure 11c). It corresponds initially to chain 1 in Figure 11 and is composed of some clustered PCLs (blue spheres in Figure 11a), connected by a flexible chain. After a certain time of

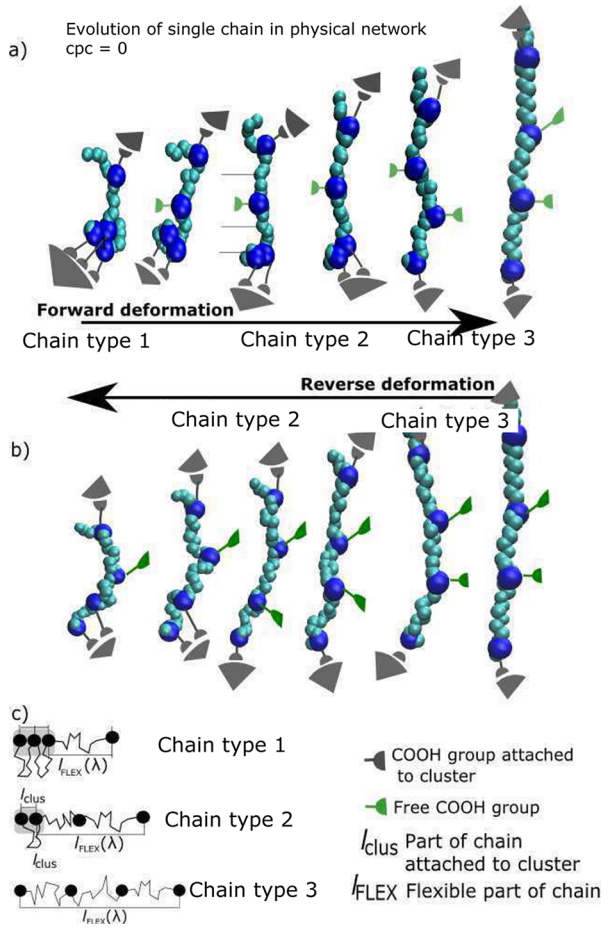

Figure 11. Evolution of a load-bearing chain from physical network during (a) forward and (b) reverse deformation. Dark blue spheres denote interacting AA groups; light blue, a flexible chain; gray, interacting groups attached to a cluster; and green, free interacting group. (c) Schematic models of combined cluster/flexible chain. Model chains 1, 2, and 3 contain 3, 2, and 1 group attached to the cluster.

steady stretching, an AA group dissociates from the big cluster, and the chain is transformed into a model chain 2. Eventually, other clustered groups dissociate, and the chain is transformed model chain 3. The structural change during the reverse deformation has been slower so that model chain 3 was transformed back to model chain 2 by reattachment of an interacting group to the cluster. The average length of the chain during this cyclic deformation between model chains 1−3 is formed by the chain fraction attached to the AA cluster and by the remaining stretched part. Note that this evolution of a chain, depicted in Figure 11, pertains to a *physical* type of network (*cpc* = 0), albeit in other networks this evolution looks similar. Solely the detachments and reattachments occur somewhat faster in covalently bound CCL−CCL chains. Their end-to-end length during the simulation changes more steadily than in the PCL chains.

The changes in the chain structures, considered above, are reflected by the chain end-to-end distance, which has been monitored during the simulation (cf. Figure 12). The end-to-end distance of certain chains in a physical networks was observed to exhibit a hysteresis rather than a smooth variation since it reflects the dissociation of AA groups from clusters. However, the data are rather scattered even when no

dx.doi.org/10.1021/ma501504z | *Macromolecules* 2014, 47, 8795−8807

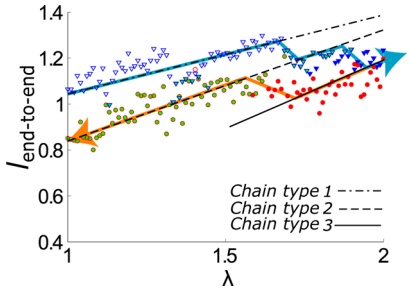

Figure 12. End-to-end length of a single load-bearing chain vs strain λ during a loading−unloading cycle: forward deformation (triangles, blue) and reverse deformation (circles, orange); lines are calculations using the schematic models 1−3 from Figure 11. The initial length of the flexible part (l_{FLEX} at $\lambda = 1$) of states 1, 2, and 3 is taken as $\sqrt{N_s}$ of the number of segments N_s: mode chain 1 has 7 segments, model chain 2 has 14 segments, and model chain 3 has 21 segments.

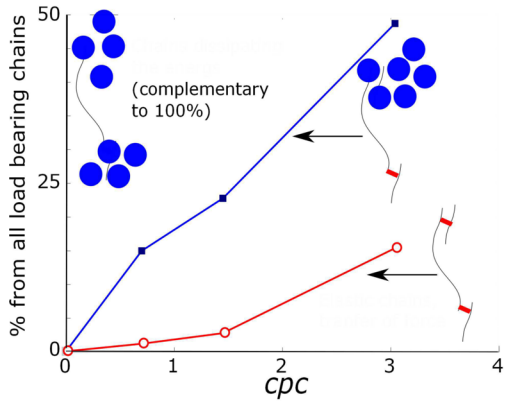

Figure 13. Classification of load-bearing chains in the simulation box: red line = percentage of chains terminated by two covalent cross-links (CCL); blue line = chains bound by combination of physical (PCL) and covalent cross-links (CCL); complementary to 100% are the remaining chains bonded by physical cross-links.

dissociation is observed. The variation of the end-to-end distances with deformation can be qualitatively understood and described by means of the schematic model chains 1−3 from Figure 11. In fact, the end-to-end distance of the chains that belong to these schematic models can be calculated. In model chain 1, two parts of the chain are attached to the cluster. Approximately, the length of such part, attached to the cluster, is $2 \cdot l_{clus}$, where l_{clus} is just the distance between two interacting AA groups in the cluster (it is an input parameter of the simulation: l_{clus} = 0.35 nm). This part of the chain which is attached to the cluster is taken as with fixed length and its length does not change during the stretching. On the other hand, the remaining part (the flexible chain) depends linearly on the stretching ratio. Therefore, the end-to-end length of model chain 1 can be calculated for the entire stretching interval (from $\lambda = 1$ to 2). For example, in model chain 2 only one part of the chain of length $1 \cdot l_{clus}$ is attached to the cluster whereas the flexible part is again linearly depending on the stretching ratio. In fact, model chain 2 demonstrates an equilibrium between dissociation and reattachment. Part of the reverse deformation can be described by the same model as forward deformation. Model chain 3 has only a single flexible part as merely the end-groups are attached to the clusters.

We have identified two structural parameters, which are related to each load-bearing chain: (i) the type of connection to the network and (ii) the network continuity. Each LBC can be connected to the complementary network by two types of cross-links which connect an end-group of the LBC to a physical cluster (PCL) or to a covalent cross-link (CCL). This leads to three possible combinations of LBC connections: chains connected by two CCLs, by two PCLs, and chains connected by a combination of one PCL and one CCL. All three types were detected in our model networks with *cpc* = 0.00, 0.70, 1.45, and 3.05 (Figure 13). The percentage of combined PCL−CCL network was found to increase linearly with increasing degree of covalent cross-linking, as expected. On the other hand, the LBCs of type CCL−CCL are present in significantly higher concentration in the strongly covalently cross-linked network as compared to the other ones. Since we know that only the strongly covalently cross-linked chains have elastic response, we can focus on the CCL−CCL chains.

There is a clear difference between inelastic ($cpc \leq 1.45$) and elastic networks ($cpc \geq 3.05$) in the *percentage of covalently cross-linked chains* (cf. Figure 13, red curve). This percentage is a parameter derived directly from the atomic configuration of the network. The parameter thus meets both our requirements (i) to correlate with the deformation response and (ii) to be directly related to to the structure that we set out.

A disadvantage of this parameter, however, is that it is quantitative and requires knowledge of the threshold fraction of CCL−CCL chains when the switch from inelastic to elastic response occurs. It would be preferable to have some qualitative criterion which decides on the character of deformation.

The second parameter was the continuity of the CCLs subnetwork (cf. Figure 14). A subnetwork (which is part of the entire network of chains) was considered continuous when it is connected by CCL−CCL chains only. The analysis of network continuity was performed in a stretched box with stretching ratio $\lambda = 2.0$.

The data were processed to histograms (Figure 14) where the horizontal axis gives the size of the subnetwork (the number of CCLs interconnected within a single subnetwork) and on the vertical axis one plots the number of such subnetworks. The total number of subnetworks is

$$y(x) = \frac{1}{4} x \sum_{i=1}^{4} N_i(x) \tag{6}$$

where x denotes the size of subnetworks (number of CCLs connected by elastic chains only), and $N_1(x)$, ..., $N_4(x)$ is the number of such subnetworks in the four independent realizations of the simulation box. $y(x)$ then characterizes the number of CCLs, which are connected to subnetworks of certain size x.

All the histograms from Figure 14 can be divided into three groups by vertical lines. Each group corresponds to different situation in the structure.

Size of Continuous Subnetworks ≤3. This type of subnetwork is mostly composed of isolated CCL chains. Occasionally, a set of three CCLs connected to one subnetwork can be found in the simulation box. This is mostly the case of lightly cross-linked chains with *cpc* = 0.7. It is evident that the chains with PCLs then play the most significant role.

Size of Continuous Subnetworks ≤7. The network forms inclusions (isles) of CCLs subnetworks in the matrix of the PCL network. A minimum of four chains is necessary to span the simulation box. However, this is accomplished only when the four chains are connected sequentially. The chains in the

dx.doi.org/10.1021/ma501504z | *Macromolecules* 2014, 47, 8795−8807

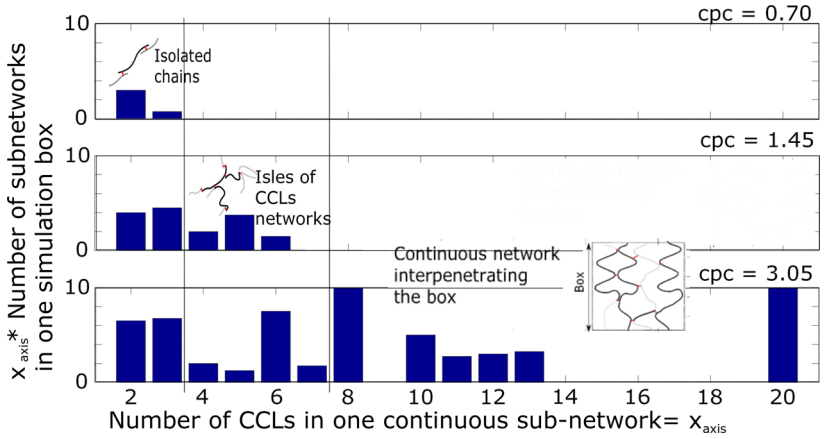

Figure 14. Histograms of continuous subnetworks of CCLs, presenting the total amount (number of CCLs) of subnetwork versus subnetwork size x. Vertical lines divide the histograms into three regions: isolated CCL chains, inclusions of CCLs in a physical network, a continuous CCLs network.

subnetworks are branched, so networks with even seven segments usually do not span the boundary of the box. The inclusions are found in the moderately covalently cross-linked network with cpc = 1.45. Also in this case, the PCLs network plays a dominant role.

Size of Continuous Subnetwork >7. In the highly cross-linked simulation box, some continuous parts of the networks connect eight and more CCLs. The subnetworks of such type exceed the boundary of the periodic simulation box. As the box is periodic, the subnetwork which spans the boundaries of box can be considered pseudoinfinite (i.e., above the percolation threshold). That case is observed in the strongly cross-linked networks with cpc = 3.05.

Apparently, the size of CCL subnetworks is the main structural property, decisive for elasticity or hysteresis. In particular, one may check if the size of such CCL subnetwork exceeds the box size. If the size of the subnetwork is smaller than the size of the box, the deformation is applied to a continuous physical network and the mechanical energy is dissipated in the physical cross-links. When the primary physical network suffers damage, such a network undergoes a spatial rearrangement without an interchange of the interacting groups.

In contrast, the deformation of a covalently cross-linked continuous network leads to the transfer of force through the covalent cross-links. Substantial force is applied to the remaining physical clusters in the network, and they dissociate quickly and easily. After the dissociation of AA groups, the force acting on an atomic group is significantly diminished and the AA group is quickly reattached to a cluster yet not necessarily at the same place. Such response is fast and without noticeable change of the potential energy.

An important aspect is the dynamic character of hysteresis. The question is whether the hysteresis disappears, when the deformation is so slow, that the changes have enough time to proceed. The dynamic aspect of structural changes is complex, and we described it elsewhere. Briefly summarized, one can divide in general the dynamic aspects into three cases:

- The first case is a strongly cross-linked (cpc = 3.05) gel, which has elastic response independently of the stretching ratio magnitude. Also, the structural changes occur relatively quickly. They are in fact faster than the shift of atomic groups due to affine deformation of the sample. The interacting groups are rather weakly attached to the clusters and can be easily detached. Therefore, the changes do not have significant influence on the deformation response.
- The second case are networks of physical type, $cpc \leq 1.45$, stretched up to λ = 2.0. In that case, several stretched macromolecules are bundled into one fibril. The fibril is difficult to disassemble by reverse deformation and the induced changes appear irreversible.
- The third case corresponds to a physical type of networks, $cpc \leq 1.45$, stretched up to deformation of $\lambda \leq 1.5$. In that case, the dynamic effect of structural recovery is observed. The networks were stretched using both slow and quick deformation rate. The quick deformation was 10 times faster than the slow one. The network was held for a while in the stretched state after quick deformation in order to match equal simulation times of both (fast and slow) simulations. Criterion for the damage was the decrease of volume fraction of PCLs in the simulation box. Damage after slow deformation was relatively small in comparison to the damage after a quick one. After the relaxation phase, in both cases damage was more or less of the same degree.

As an indicator of structural recovery we have used in a recent work the return of cluster volume fraction to the state before deformation. Recovery is thus a process opposite to network damage whereby a decrease of cluster volume fraction also takes place. Recovery has usually been observed within a time interval from nanoseconds to tens of nanoseconds, and for all networks it follows almost the same course.

In this study we analyzed to what extent the hysteresis depends on dynamics, or it disappears when static loading is performed. For the analysis the same functions as in Figure 5 were examined, although the simulation was carried out as a static deformation. In real experiments, such static loading is usually applied in several steps whereby each step is followed by a long period of relaxation. In our simulations such an approach would take, however, much computer time. Instead, we followed a different procedure, using time intervals of equal duration 10 ns, during which the system was deformed up to λ = 1.1, 1.2, 1.3···2.0. At the end of each such interval, the AA clusters were let to disintegrate by switching off the interactions between AA units. Then, after another period of 10 ns deformation, the interactions between AA units were switched on again, and the AA units formed clusters again. These newly formed clusters are thus created in equilibrium, yet no changes in structure were observed.

dx.doi.org/10.1021/ma501504z | Macromolecules 2014, 47, 8795−8807

The energy variation during such static treatment is presented in Figure 15. The behavior of network with *cpc* =

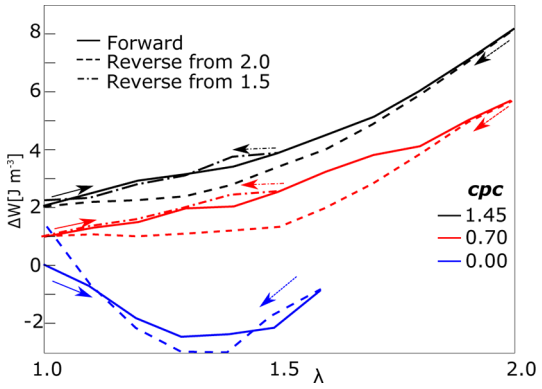

Figure 15. Energy density as a function of stretching ratio λ. Forward and reverse deformation in static mode for different degree of cross-linking (for comparison with quick deformation, see Figure 5).

0 during static deformation has unphysical nature. The energy decreases during increasing deformation in the first phase. This is an artifact caused by the annihilation and the subsequent reappearance of clusters. The simulation box should grow in volume, when the clusters disintegrate. However, the volume increase of the box was restricted by model settings, generating pressure at the box boundaries. This pressure acts together with deformation. The dynamic behavior under static loading can be investigated only for *cpc* = 0.70 and 1.45, where no change in volume is observed. It was then found that no hysteresis up to stretching ratio λ = 1.5 was observed. The hysteresis produced by stretching up to λ = 2.0, instead, does not disappear but is only decreased. Therefore, the results under static deformation are in agreement with the general dynamic behavior, outlined in the itemized list above. The creation of irreversible fibrillar structures at high deformation is also observed in the static mode.

CONCLUSIONS

We have investigated the deformation behavior of double-network gels with reversible physical and irreversible covalent cross-links using molecular dynamics simulation. We found that the appearance of hysteresis during the loading−unloading cycles depends on the molecular structure of the gels.

Apparently, the amount of disentanglement and rupture of the primary network looks similar for all investigated networks, albeit the damage mechanism may be different. The networks with hysteresis show rather slow reconstruction of physical clusters whereas the elastic networks exhibit quick segmental hops between physical clusters. The overall degree of nonaffine deformation was similar for all the model networks; however, a significant difference was observed between networks with predominantly physical or covalent cross-links.

We have identified the properties of load-bearing chains (LBCs) as a crucial structural factor, which correlates with the degree of elasticity and can be immediately derived from the simulation. The variation of the elastic energy of load-bearing chains was found to comply remarkably well with the elastic energy variation of the entire sample. The type of tethers, connecting the LBCs to the rest of the network, by virtue of an either covalent or a physical interaction, plays a significant role. The continuity of subnetworks, composed of covalent cross-links only, was another important structural variable affecting the character of the deformation response.

The proposed model, therefore, appears to provide ample insight into the relationship between gel structure and performance and could be used in the development of self-healing hydrogels for engineering and medical applications.

ASSOCIATED CONTENT

Supporting Information

Extension of Figures 2 and 10. Figure 2 in this paper presents the basic configuration of dry phase of network and selected atoms in dry phase. The supporting material presents also full configuration of box with water. Next, there is a detail of part of chains with water molecules. All the configurations are presented also in real 3D format, which enables one to observe atomic configuration in real 3D volume. One can have detailed picture about physical clusters and alternatively distribution of water molecules around the chains (details of water around single chains.) The first 3D format ANAGLYPH can be shown on standard screens with red-cyan glasses. Next 3D format is VISION LIVE (.jps) file. It can be shown on special types of screen (3D-screens, TVs, tablets, and smartphones). Figure 10a,b in this paper is an output from simulation completed by illustration. The movie presented in supporting materials shows the untreated output from simulation. It shows also development of single chain in time. Next Supporting Information (supplementary 3) shows movie with deformation of three networks with different degrees of cross-linking. Differences in network structure are highlighted. This material is available free of charge via the Internet at http://pubs.acs.org.

AUTHOR INFORMATION

Corresponding Author

*E-mail jan.zidek@ceitec.vutbr.cz; Ph +420 5 41149456; Fax +420 5 41149361 (J.Z.).

Notes

The authors declare no competing financial interest.

ACKNOWLEDGMENTS

J. Zidek and J. Jancar acknowledge the European Regional Development Fund (CEITEC, CZ.1.05/1.1.00/02.0068).

REFERENCES

(1) Michlovska, L.; Vojtova, L.; Mravcova, L.; Hermanova, S.; Kucerik, J.; Jancar, J. *Macromol. Symp.* **2010**, *295*, 119−124.
(2) Lee, S.; Kim, Y. L. J. E.; Park, T. G.; Ahn, C.-H. *J. Mater. Chem.* **2009**, *19*, 8198−8201.
(3) Park, C.; Kim, S. *J. Polym. Sci., Part A: Polym. Chem.* **2010**, *48*, 1287−1297.
(4) Hao, J.; Weiss, R. *Macromolecules* **2011**, *44*, 9390−9398.
(5) Bossard, F.; Aubry, T.; Gotzamanis, G.; Tsitsilianis, C. *Soft Matter* **2006**, *2*, 510−516.
(6) Tamai, Y.; Tanaka, H.; Nakanishi, K. *Macromolecules* **1996**, *29*, 6750−6760.
(7) Wu, R.; Li, T.; Nies, E. *Macromol. Theory Simul.* **2012**, *21*, 250−265.
(8) Hao, J.; Weiss, R. *ACS Macro Lett.* **2013**, *2*, 86−89.
(9) Nakayama, A.; Kakugo, A.; Gong, J. P.; Osada, Y.; Takai, M.; Erata, T.; Kawano, S. *Adv. Funct. Mater.* **2004**, *14*, 1124−1128.
(10) Myung, D.; Koh, W.; Ko, J.; Hu, Y.; Carrasco, M.; Noolandi, J.; Ta, C.; Frank, C. *Polymer* **2007**, *48*, 5376−5387.
(11) Peak, C.; Wilker, J.; Schmidt, G. *Colloid Polym. Sci.* **2013**, *291*, 2031−2047.
(12) Gong, J. *Soft Matter* **2010**, *6*, 2583−2590.

(13) Gilormini, P.; Diani, J. *C. R. Mec.* **2012**, *340*, 338−348.
(14) Yang, C.; Wang, M.; Haider, H.; Yang, J.; Sun, J.-Y.; Chen, Y.; Zhou, J.; Suo, Z. *ACS Appl. Mater. Interfaces* **2013**, *5*, 10418−10422.
(15) Schmoller, K.; Bausch, A. *Nat. Mater.* **2013**, *12*, 278−281.
(16) Xia, L.-W.; Xie, R.; Ju, X.-J.; Wang, W.; Chen, Q.; Chu, L.-Y. *Nat. Commun.* **2013**, *4*, 2226.
(17) Jiang, F.; Huang, T.; He, C.; Brown, H.; Wang, H. *J. Phys. Chem. B* **2013**, *117*, 13679−13687.
(18) Li, Y.-L.; Ouyang, N.; Ke, A.-R.; Lin, S.-B. *J. Appl. Polym. Sci.* **2013**, *128*, 761−766.
(19) Costa-Junior, E.; Barbosa-Stancioli, E.; Mansur, A.; Vasconcelos, W.; Mansur, H. *Carbohydr. Polym.* **2009**, *76*, 472−481.
(20) Webber, R. E.; Creton, C.; Brown, H. R.; Gong, J. *Macromolecules* **2007**, *40*, 2919−2927.
(21) Sun, J.-Y.; Zhao, X.; Illeperuma, W. R. K.; Chaudhuri, O.; Oh, K. H.; Mooney, D.; Vlassak, J.; Suo, Z. *Nature* **2012**, *489*, 133−136.
(22) Brown, H. *Macromolecules* **2007**, *40*, 3815−3818.
(23) Tanaka, Y. *Europhys. Lett.* **2007**, *78*, 56005.
(24) Baumberger, T.; Caroli, C.; Martina, D. *Eur. Phys. J. E: Soft Matter Biol. Phys.* **2006**, *21*, 81−89.
(25) Okumura, K. *Europhys. Lett.* **2004**, *67*, 470−476.
(26) Tirumala, V.; Tominaga, T.; Lee, S.; Butler, P.; Lin, E.; Gong, J.; Wu, W.-L. *J. Phys. Chem. B* **2008**, *112*, 8024−8031.
(27) Hui, C.-Y.; Long, R. *Soft Matter* **2012**, *8*, 8209−8216.
(28) Peleg, O.; Savin, T.; Kolmakov, G. V.; Salib, I. G.; Balazs, A. C.; Kroger, M.; Vogel, V. *Biophys. J.* **2012**, *103*, 1909−1918.
(29) Zidek, J.; Milchev, A.; Vilgis, T. *J. Chem. Phys.* **2012**, *137*, 244908.
(30) Humphrey, W.; Dalke, A.; Schulten, K. *J. Mol. Graphics* **1996**, *14*, 33−38.
(31) Miyamoto, S.; Kollman, P. *J. Am. Chem. Soc.* **1992**, *114*, 3668−3674.
(32) Hess, B.; Kutzner, C.; van der Spoel, D.; Lindahl, E. *J. Chem. Theory Comput.* **2008**, *4*, 435−447.
(33) Bussi, G.; Donadio, D.; Parrinello, M. *J. Chem. Phys.* **2007**, *126*, 014101.
(34) Huisman, E.; van Dillen, T.; Onck, P.; der Giessen, E. V. *Phys. Rev. Lett.* **2007**, *99*, 208103.
(35) Broedersz, C. P.; Sheinman, M.; MacKintosh, F. C. *Phys. Rev. Lett.* **2012**, *108*, 078102.
(36) Head, D.; Levine, A.; MacKintosh, F. *Phys. Rev. E* **2003**, *68*, 061907.
(37) Hatami-Marbini, H.; Picu, R. C. *Phys. Rev. E* **2008**, *77*, 062103.
(38) Kurniawan, N.; Wong, L.; Rajagopalan, R. *Biomacromolecules* **2012**, *13*, 691−698.
(39) Treloar, L. *The Physics of Rubber Elasticity*, 3rd ed.; Clarendon Press: Oxford, 2005.
(40) Floyd, R. W. *Commun. ACM* **1962**, *5*, 345−348.
(41) Warshall, S. *J. Assoc. Comput. Mach.* **1962**, *9*, 11−12.